International Journal of Research in Engineering and Science (IJRES)
ISSN (Online): 2320-9364, ISSN (Print): 2320-9356
www.ijres.org Volume 10 Issue 10 ǁ October 2022 ǁ PP. 167-179

Autonomous Street Lighting System Based on Solar Energy and LED'S

Anil Singh[1], Er. Virender Lohan[2]
[1]*M.Tech. Student of Electrical Engineering, Department of Electrical Engineering, JIET, Jind-136119, Haryana., INDIA*
[2]*Assistant Professor of Electrical Engineering, Department of Electrical Engineering, JIET, Jind-136119, Haryana., INDIA*

Abstract:- *Currently, two types of solar panels are in use. Fixed panels have a fixed tilt angle and are installed at a convenient angle based on the geographical location. However, irradiation time is only six hours per day. The second type is revolving panels, which track the sun continuously or rotate at a predetermined angle at a certain period. Unfortunately, both continuous tracking and pre-programmed techniques are ineffective. In the first, a low-speed motor necessitates a high torque, which necessitates a high current, resulting in increased driving power. The system rotates at specified tiny angles in the second method, regardless of whether the new position adds to extra energy or not. In fact, it's possible that the extracted energy will be absorbed entirely by the driving mechanism. This research demonstrates a new technique that addresses those two flaws.*
To maximise solar energy extraction, the design employs a microcontroller-based control system. This is accomplished through the development of the PILOT tracking system and the PANEL cell rotation system. To begin, the system is directed eastward, waiting for the sun to rise. When this occurs, the PILOT continues to monitor the sun. A light to frequency converter (LTF) installed on a small electric motor is used to do this. This converter aligns the PILOT with the sun at all times. One on the PILOT and the other on the PANEL, two identical light dependent resistors (LDR) are installed. A comparing mechanism takes over after each PILOT placement. The PANEL aligns itself with the PILOT if the voltage generated by the PILOT LDR is larger than the voltage induced by the PANEL LDR plus a predetermined offset; otherwise, it stays in its present position and waits for the PILOT to move to a new location, and the process repeats. The PANEL will only move to the new position if the latter produces more energy. After the sun sets at the end of the day, the system returns to its original location and waits for the next day.
Key words:- *Solar cell, PANEL, PILOT, PIC microcontroller, LDR, LTF*

Date of Submission: 23-09-2022 Date of acceptance: 06-10-2022

I. INTRODUCTION

One of the most pressing concerns for the next half-century is finding energy sources to meet the world's expanding demand. Global warming and unpredictable climate variations have been driven by the greenhouse effect in recent years. Few countries still rely on fossil fuels to generate power, which emit greenhouse gases that have serious consequences for human and wildlife populations. Pollution and the rising expense of fossil fuels around the world have prompted many to focus on renewable energy sources. According to scientific forecasts, fossil fuel use will drop by 80% while non-fossil fuel consumption will rise by 50% during the next 30 years. According to statistics, available fossil fuels will be depleted by 2080. As a result, non-conventional energy sources must be the dominant energy source [21]. The sun provides the earth with 16x1018 units of energy every year, which is 20,000 times the amount of energy required by people on the planet [22]. On a sunny day, the sun emits roughly 1 kW/m2 of energy. "The International Energy Agency projects that nearly one-quarter of renewable energy, or 11% of global electricity, might be supplied by solar energy in 2050," according to [23]. As a result, the goal of this study is to improve solar energy harvesting by creating and constructing an autonomous microcontroller-based solar tracker with a hybrid algorithm that can precisely find the sun's position. Experiments were carried out to assess the suggested solar tracker's performance in the context of the local climate. A webpage was also created to aid in the timely monitoring of solar data.

1.2. Electrical generation from solar cells

A photovoltaic cell, often known as a solar cell, is used to convert solar energy into electrical energy. Solar cells are made up of silicon-like semiconductors, and a PV solar panel is made up of a large number of solar cells. One layer of the cell is commonly doped with Boron or any trivalent impurity (p-type semiconductor) to promote a positive charge, while the other layer is doped with Phosphorous or any pentavalent impurity to facilitate a negative charge (n-type semiconductor).

When these two different types of semiconductors are combined, they form a PN junction. Near the surface, concentration gradients of electrons and holes cause holes to diffuse from p-type to n-type and electrons to diffuse from n-type to p-type (Fan et al., 2018). When photons from the sun collide with silicon electrons in solar cells, some of the photons' energy is transferred to the silicon electrons, and this energy is large enough to separate the electrons from their parent silicon atom. Within the n-type silicon, free electrons travel and gather. The electrodes are connected to the external circuit, and the electric current is generated by the movement of electrons from n-type to p-type through the electrodes and the external circuit (cosmos magazine, 2017).

Near the surface, concentration gradients of electrons and holes cause holes to diffuse from p-type to n-type and electrons to diffuse from n-type to p-type. When photons from the sun collide with silicon electrons in solar cells, some of the photons' energy is transferred to the silicon electrons, and this energy is large enough to separate the electrons from their parent silicon atom. Within the n-type silicon, free electrons travel and gather. The electrodes are connected to the external circuit, and the electric current is generated by the movement of electrons from n-type to p-type through the electrodes and the external circuit.

1.3 Types of PV systems

Solar PV and Storage Systems are classified Into Three Types-

• Grid tied or grid Direct PV System
• Off Grid PV System
• Grid/Hybrid or Grid — Interaction System with Energy Storage

1.3.1. Grid tied or grid-direct PV system

This is a simple solar system with a grid-tied inverter. There is no battery bank for storage in a grid-connected solar PV system. Only during the day can power be generated and used from a grid-tied system. This system is extremely cost-effective, easy to construct, manage, and requires minimal maintenance. Figure 1 depicts a schematic illustration of the system. The fundamental goal of a grid-tied system is to reduce energy costs. Solar panels typically produce more electricity than the loads require. As a result, instead of storing the excess electricity in the batteries, it can be returned to the grid. Additionally, some additional cash can be earned by selling the solar panel's excess generated power, lowering the LCOE even further (levelized cost of energy of system) Because the PV panels create DC electricity, an inverter is required to convert the DC to AC.

The grid-direct system's disadvantage is that it can only be used during the day. Power cannot be saved for future use, such as in the event of a power outage. This drawback can be avoided by utilising a battery bank to store the generated power throughout the day, but this new setup will raise the system's cost in the long run.

1.3.2. Off grid solar PV system

Customers who have difficulty connecting their load to the grid will benefit from this method. Batteries are used in off-grid solar PV systems to store electricity generated during the day so that it can be used later or in an emergency (such as a cloudy day) and at night. When building this system, year-round conditions and weather fluctuations must be taken into account. Back-up generators are required if the sun does not shine for several days in a row or if snow accumulates on the PV panels. The generator can run on gasoline, diesel, petroleum, or propane. The AC output of backup generators can be used directly or converted into D.C. for storage in batteries. Figure 2 depicts a schematic illustration of the system. This system has the advantage of providing enough energy for a home while also being able to power locations that are off the grid. Off-grid systems feature additional components and are therefore more expensive and costly than grid-direct systems.

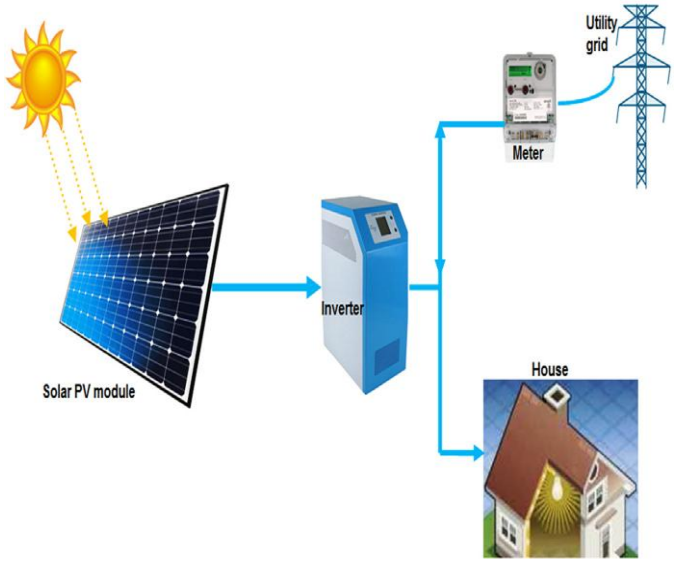

Fig. 2. Grid tied/direct PV system.

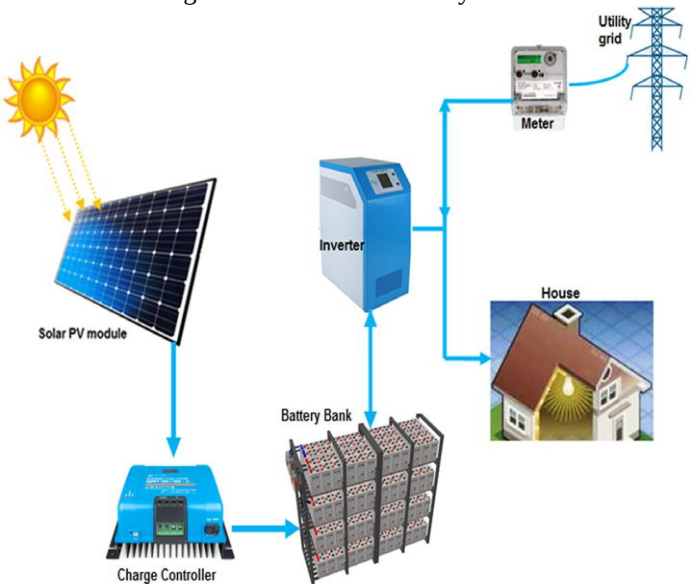

Fig. 1. Off grid PV system.

1.3.3. Grid interactive system

Customers who are currently connected to the grid but desire a battery backup will benefit from this technology. The advantages of both grid-direct and off-grid systems are combined in this system. Through extensive incentives, this approach can assist in cutting utility bills. However, this grid system isn't just for incentive programmes; if there's a power outage, the energy from the battery bank can be used in an emergency (Solarpowerworldonline, 2015). During high demand, the batteries' stored energy can also be used. When sensors are deployed to detect the position of the sun, which is then feed-backed to the system so that the comparator/microprocessor used in the system can detect the error and give the required actuating signal to the motors to correct the error, the algorithm is based on mathematical calculations based on the sun's trajectory. The system is then considered to be operating on feedback control principles. Closed loop solar trackers are the trackers that use the above-mentioned technology.

Sensors assess the amount of radiation and operate the motors accordingly.

II. LITERATURE REVIEW

Solar PV technologies, which use solar energy to generate electricity, have been quickly accelerating in recent years as an effective solution to the global energy crisis and the problem of environmental pollution. To address the ever-increasing market need, many types of solar cells based on innovative materials are developing [1]. From first-generation Si wafer-based solar cells (e.g., m-Si and polycrystalline Si solar cells) to second-generation thin-film solar cells, the evolution of solar cells has been rapid (e.g., a-Si, CIGS, and CdTe solar cells) to the more

modern third-generation solar cells (e.g., dye-sensitized, organic, and perovskite solar cells) [2], which are based on innovative light-absorbing materials. First-generation solar cells based on established crystalline Si-based technology, in particular, have demonstrated significant stability, scalability, cost effectiveness, and efficiency in commercial applications.

According to **Yoshikawa et al**. [3], the PCE of crystalline Si heterojunction solar cells can exceed 26%. and MacQueen et al. [4] identified a key path toward improving the PCE of single-junction crystalline Si-based solar cells in the near future, i.e., closer to the Shockley–Queisser limit (30 percent at a band gap of 1.1 eV), which defines the maximum theoretical limit of solar energy conversion [5]. m-Si solar cells with PCEs of above 20% are commonly accessible in the commercial market, for example, from SunPower (SPR-X22-370) and LG (LG360Q1C-A5).

Benick et al. [6] demonstrated in 2017 that polycrystalline Si solar cells can attain a high PCE of around 22.3 percent. Due to structural inhomogeneity [7] and light-induced deterioration in terms of dangling bond density [8], the PCEs of second-generation a-Si thin-film solar cells are still lagging behind those of first-generation solar cells. The PCE of hydrogenated a-Si thin-film solar cells remains at 12.69 percent, as shown in [9]. In the visible-light spectrum, however, the light absorption coefficient of a-Si thin-film solar cells is higher than that of crystalline Si-based solar cells, allowing them to respond better to weak visible light [8]. Furthermore, due to their minimal material use, great flexibility, cheap cost, and light weight, second-generation a-Si thin-film solar cells based on thin film technology can better penetrate the consumer electronics sector. With the advancement of materials and processing technology in recent years, second-generation solar cells based on CIGS and CdTe have attained PCEs of 22.9 percent and 21%, respectively [10]. This is due to the fact that in the longer wavelength portion of the solar spectrum, i.e., 700–900 nm, both CIGS and CdTe solar cells exhibit larger absorption coefficients than a-Si thin-film solar cells [11]. However, the utilisation of rare earth elements in both types of solar cells, as well as their hazardous nature, remain substantial barriers to their practical application. Third-generation solar cells based on innovative materials, such as dye-sensitized, organic, and perovskite solar cells, have been quickly developed over the last ten years as a result of material improvements. Although low-temperature solution-processed perovskite solar cells still have stability difficulties,

Jiang et al. [12] reported a record-high PCE of up to 23.7 percent in 2017, bringing the field closer to mature Si-based technology. Oxford PV announced a PCE of up to 28 percent in late 2018 [13]. These records, set with perovskite-based materials, outperform many crystalline Si solar cell records. Despite their simplicity of fabrication, the maximum PCEs achieved for organic and dye-sensitized solar cells, 11.2 percent and 11.9 percent, respectively, are lower than those for perovskite-based materials [10].

According to Roche [26], a fenestration system combined with an autonomously controlled blind has the potential to save a significant amount of lighting energy while also providing a pleasant visual experience.

So-Hyun Kim et al. [27] suggested a daylight responsive dimming-PV blind LED lighting system in a test room. This shading system is distinguished by the simultaneous energy savings and generation of power from electrical illumination. Controlling the slat angles of PV blinds to be perpendicular to the sun's profile angles resulted in around 35 percent energy savings and a 32 percent increase in power generation. When compared to a fixed slat angle control,

According to **Koo et al.** [23], incorporating an automated rotation control mechanism into a blind is more helpful for increasing the amount of daylight that enters the building interior. Both the energy saving potential and the degree of daylight input could be greatly increased by adjusting the blinds automatically. Many researchers have examined and studied the sun-tracking blind-window system, whose slats are rotated in response to the solar position, to overcome various shortcomings of shading devices in terms of low efficiency of daylighting performance and sunlight glare. Many investigations on photovoltaic systems under sun-tracking control with two-[28] or three-direction-of-automatic-rotation [29] have been published. to now, however there have been very few investigations on shading devices. [30] To allow the blind slats to be rotated in more than one direction, they To make a rectangle matrice, it should be cut vertically or horizontally.

Jayathissa et al. [31] suggested an optimal sun-tracking control approach for shading panels and investigated all potential dynamic shading panel orientations. In terms of cooling and heating loads, the research found that a 20–80 percent energy savings was achieved when compared to an identical alternative consisting of static shade panels. However, for ease of calculation, all of the panels were turned in 15° increments at the same time, according to the position of the sun. As a result, the shade panels cannot follow a continuous sun-tracking movement trajectory using this method.

Gao et al. [30] created a building model that is integrated with the window system's sun-tracking shading panel array. The solid analytical geometry mathematically described the one-degree-of-freedom, two-degree-of-freedom, and variable-pivot-three-degree-of-freedom sun-tracking control systems. The computed findings demonstrate that variable-pivot-three-degree-of-freedom sun-tracking is the best control approach for shade panel arrays, resulting in a 19.17 percent increase in annual lighting energy efficiency.

Song et al. (2014) suggested an optical fiber-based day lighting system using a solar tracking model. Because the tracking precision is better than 0.1 degree, the amount of overlap between the focal spot and the entrance face is greater than 80%. The system is made up of 2500 suns of concentration. The device consists of two feedback loops, coarse and fine adjustments, and the system performs well in terms of tracking. The optical transmission efficiency is between 37% to 40%, which is close to the theoretical value of 42%.

Sungur (2009) used a programmable logic controller unit to create a dual-axis solar tracking device. The PLC programme was implemented using azimuth and altitude solar angle calculations, in which the sun's azimuth and altitude angles were determined over the course of a year, at each hour of the day. The tracking mechanism was guided by the calculated slope angles. The PLC programme gave analogue signals to the motors based on the azimuth and altitude angle computations, ensuring that the PV panel remained normal to the sun's radiations. When compared to a fixed solar model with similar output statistics, the dual-axis solar tracking system produced 42.6 percent more energy.

Barker et al. (2013) suggested a low-profile 2-axis solar tracker with a unique connection design to reduce shadowing from nearby trackers. To keep solar tracker installation costs down, the device was fastened to the ground with ground screws. Two coplanar and perpendicular linear actuators were coupled with a single linkage arm and pivots in the design. And while this was tested in order to improve grid packing density in order to maximise production, no significant difference in shadow footprint was noticed when compared to existing mast-style trackers.

III. WORKING PRINCIPLE

Thousands, if not millions, of photovoltaic cells are required to extract energy from the sun. This is feasible in our region, which has plenty of room and energy. As previously stated, a fixed panel is not an option, and moveable panels must be carefully considered. The method provided here is for the creation of an optimal panel positioning mechanism that extracts maximum energy with little panel movement, regardless of weather conditions or the length of the day for different seasons, and consumes the least amount of energy achievable by the motors. Irradiation will undoubtedly be reduced on cloudy or rainy days, whether fixed or moving panels are used; however, the proposed system is unaffected because it recovers and aligns itself properly even in these extreme conditions thanks to the light detector, which allows the system to rotate back if necessary. However, in Bahrain, where it rarely rains, this is not a huge issue.

There are two sub-mechanisms in the scheme. The first sub-mechanism, known as the PILOT, is responsible for locating the location where the most energy may be harvested, while the second sub-mechanism, known as PANEL, is made up of solar panels. A search approach based on the PILOT scheme is used to determine the position. The PILOT is based on a small sensor that is mounted on a little electric motor that uses very little power. Figure 3 depicts the tracking system. Three synchronised detectors, one of which is the TSL235R light to frequency converter (LTF), and two LDRs, establish the best irradiation position. On a single monolithic CMOS integrated circuit, the LTF combines a photodiode and a current to frequency converter. It generates a square wave with a 50:50 duty cycle and a frequency proportional to the light intensity (irradiation). The device was meant to respond throughout a wavelength range of 320 nm to 1050 nm, according to the chip datasheet (2007).

There are three major benefits to using the device. It does not require any additional electronics. It's simple to connect to a microcontroller, and it's simple to programme to monitor the sun. The LTF is attached to the centre tip of the W shape stand, with the two LDRs in the shape's troughs on either side. The system functions according to the following chronology. Both PANEL and PILOT point to the geographical east and wait for the sun to rise. A proximity switch known as the Start proximity switch determines their position for synchronisation purposes. (refer to Fig. 3). The PILOT's mission is to track the sun autonomously. The sun is tracked with the use of a light to frequency converter sensor (LTF). The LTF monitors the irradiation by converting it into frequency as the sun moves along its orbit. As a result, the PILOT follows suit until the maximum frequency is achieved, at which point it comes to a halt. A comparison of the induced voltage of the PILOT with the voltage induced at the previous position of the PANEL through two identical LDRs, one mounted on the PILOT and the other on the PANEL, is performed on each movement of the PILOT. Figure 4 depicts this. The output of the comparator goes high if the PILOT sensor voltage is greater than that of the PANEL by a preset offset value (the offset is programmable, so it could be set to any convenient value), indicating that the new location has a better energy extraction, interrupting the microcontroller to guide the PANEL to align itself with the PILOT. It comes to a halt until a switch positioned on the inside wall of the tube containing the PILOT is activated. The switch is nothing more than a micro limit switch mounted on the inside wall of the hollow pedestal that houses the PANEL. When the PANEL is triggered, it rotates until it is near the PILOT, where a little pin installed on the rod carrying the PILOT activates the macro-switch. After that, the PANEL comes to a complete stop. If the comparator does not go high, showing that the new position does not contribute more energy extraction, the PANEL returns to its previous position, the PILOT resumes the search, and the operation repeats itself. Three sensors are installed on the PILOT for successful tracking: two LDRs and one TSL235R light to frequency converter. The left LDR's duty is to locate the sun when it is on the left side, so

the PILOT spins to the left, and the right sensor's role is to locate the sun when it is on the right side, so the PILOT revolves to the right, as illustrated in Fig. 3.

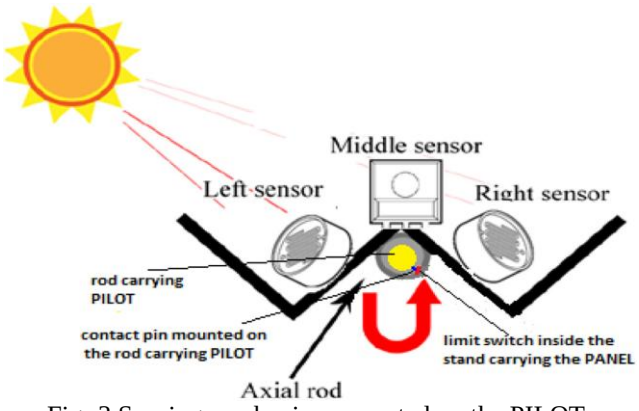

Fig- 3 Sensing mechanism mounted on the PILOT.

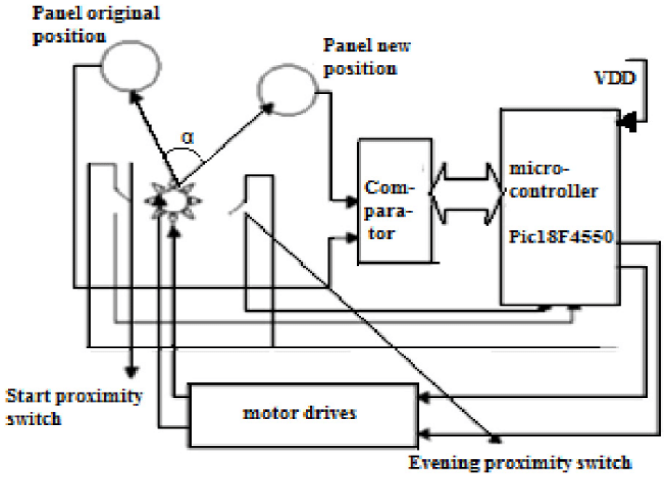

Fig- 4 Tracking system for maximum sun inclination angle.

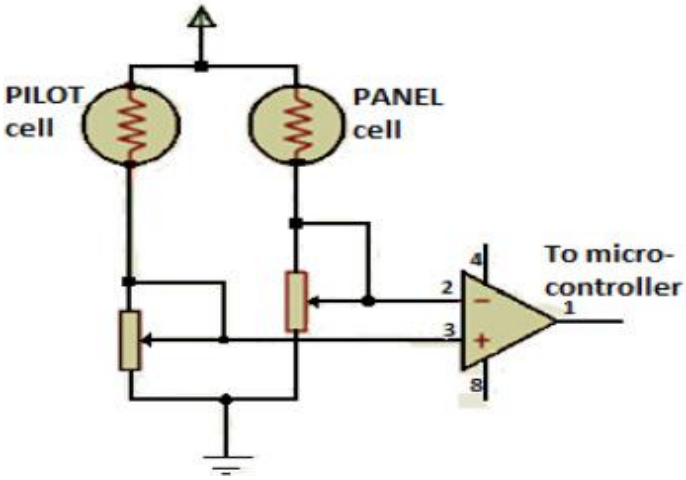

Fig- 5 Detection of voltage difference between PILOT LDR voltage and PANEL LDR voltage.

The middle sensor (TSL235R) ensures that the PILOT is always facing the sun by translating the highest possible irradiance into the highest possible frequency. This technique is especially beneficial on cloudy days because it allows the system to distinguish between irradiation dimming due to misalignment and irradiation dimming due to clouded sky. If the PILOT is in synchronism with the sun and the clouds clear, it keeps tracking; if the PILOT has advanced the sun, it compensates by rotating back and aligning itself with the sun, as does the PANEL. Fortunately, clouds only come for a few days each year in our region of the planet. According to weatherspark, the sky is clear more than 93 percent of the time, leave alone rain, with only 9.9 days of rain per year

(Light of frequency, 2007). As a result, the cloud isn't a major concern. The tracking system has accounted for the difference in day length between seasons by ensuring that the system never passes over the sun, regardless of the day length. However, in the event that the tracking fails, a limit switch known as the evening switch is set at 180 degrees from the start, directly facing the geographical west.

This is so that the system does not overshoot the trajectory on shorter days. When the PILOT presses the switch, the entire system grinds to a halt and waits for the sun to set. When this occurs, the entire system rotates back to face east and waits for the next day, at which point the operation repeats itself. The system's appeal is that it only takes one PILOT to power a vast number of solar cells. The chronology of the tracking system during the complete day, including the possibility of foggy days, is depicted in Fig. 6 and the flowchart below.

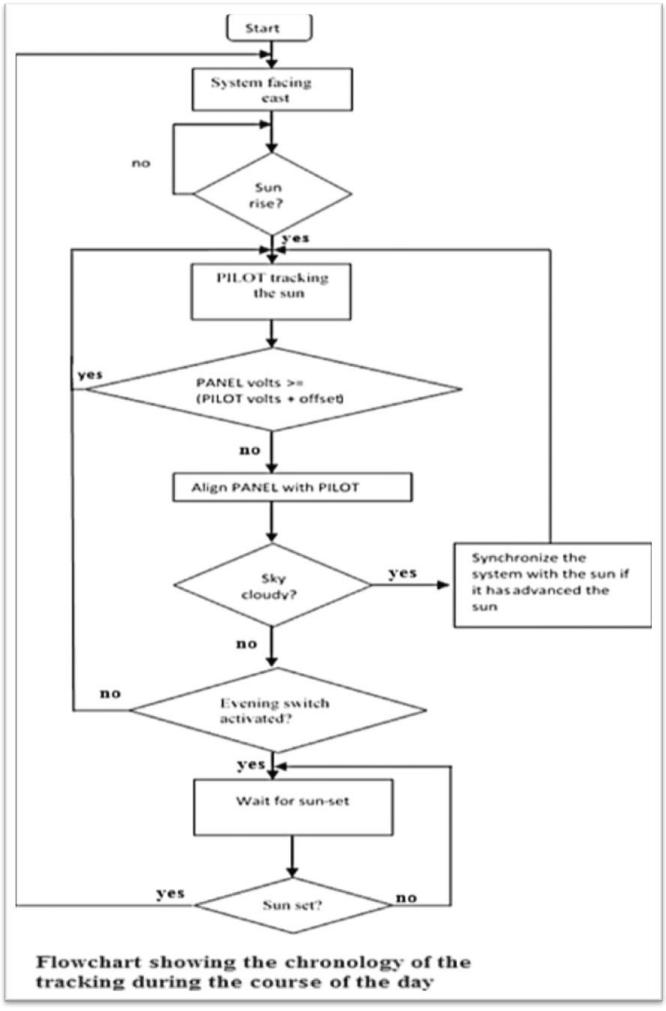

Fig- 6 The chronology of the tracking system

In this design, the crank mechanism was used to convert rotational momentum into linear motion. Instead, more efficient linear actuators would be used in future design ideas. All moving parts on the solar tracker need to be serviced once a year. Basic checks to ensure that everything was working properly, as well as lubrication to prevent friction, which would otherwise lower the motor's efficiency. The stow-angle is the parking position in the event of severe weather, and the control system must be set to accommodate it. The most common winds in the country, as well as their speeds and directions, must be determined. This information aids in determining the solar tracker's best stow angle. Some of the prototype's joints only had one degree of freedom and could only move in one direction. This was a concern since it created friction and interfered with the solar tracker's planned movement. The introduction of universal joints, which allowed for unidirectional movement, solved this difficulty. While the solar tracker was successfully conceived and produced using locally accessible materials, the model's design could be modified to increase efficiency and reduce manufacturing costs. Mild steel was mostly employed in the construction of this solar tracker. While mild steel has several qualities that make it perfect for a solar tracker, the major difficulty was the weight, which limited movement and rotation for the tracker's intended use. The greater the torque, the heavier the material, and thus a motor capable of withstanding that torque was required. This had a negative impact

on the final product's costing. Although aluminium is a viable alternative, it was significantly more expensive than mild steel. Alternatively, used and probably less expensive aluminium might be utilised to build the frame. Because it can only track the sun in one direction, it is confined to seasonal tracking. The addition of a wedge would eliminate this limitation by allowing the tracker to move in two dimensions. This would also help to narrow the gap between theoretical and calculated efficiency gain figures. The user can operate the solar tracker using a remote control without coming into contact with the motor. This is possible through the usage of mobile phones. Mobile applications can be specifically designed and developed to control the panel. A wireless signal would be used to communicate between the mobile phone and the microcontroller. The user would be able to enter the appropriate inputs using his or her mobile phone, as well as view the power output and other values of the user's choosing.

IV. DESIGN AND IMPLEMENTATION

4.1 Electromechanical system *:-* As shown in Fig. 1, the proposed solar tracker includes light dependent resistors (LDRs), an Arduino mega microcontroller, an Arduino Wi-Fi shield, a servo motor, a stepper motor and driver, an HMC5883L magnetometer, an ACS712 current sensor, and a solar panel with a supporting metallic servo bracket (a). This electromechanical system comprises of two stepper motor and servo motor drivers, with the former spinning in north and south directions and the latter revolving in east and west directions. The solar panel generates a voltage proportionate to the intensity of the sunshine, while the LDRs detect system misalignment and provide signals to the microcontroller, which adjusts the motors to rectify the solar panel position automatically.

Fig- 7 the solar panel position automatically.

4.2 Hybrid algorithm for solar tracking

In solar tracking, active and chronological algorithms are frequently used. The active algorithm is a closed-loop tracking system based on the feedback control principle. The system controller receives data from a light sensor that detects the brightness of the sun. The chronological algorithm, on the other hand, controls the movement of the solar panels by recognising the sun's motion using sun tracking mathematical models [5, 6]. The microprocessor calculates the sun's location and uses established azimuth and elevation angles to drive motors to move the solar panel towards the sun at predetermined time intervals. The azimuth angle is the horizontal angle measured from true north to the horizontal projection of the sun beam, as defined by Equation (1) [1], where is the location's latitude, is the solar declination angle, and denotes the hour angle. The azimuth angle is the horizontal angle measured from true north to the horizontal projection of the sun beam, as defined by Equation (1) [1], where is the location's latitude, is the solar declination angle, and denotes the hour angle.

$$\text{Azimuth angle} = \tan^{-1}\left[\frac{\sin\theta}{(\cos\theta\sin\varphi)-(\tan\delta\cos\varphi)}\right] \qquad (1)$$

The elevation angle, on the other hand, is the angular height of the sun in the sky as measured from the object's horizon. As shown in Equation 2 [5, 6], the elevation angle fluctuates throughout the day based on the day of the year and the latitude of that particular site. The historical solar track may not precisely determine the sun's position due to the complexity of sun movement.

$$\text{Elevation angle} = \sin^{-1}\left[(\sin\delta\sin\varphi)+(\cos\delta\cos\varphi\cos\theta)\right] \qquad (2)$$

We present a hybrid approach that combines active and chronological algorithms to increase overall solar tracking accuracy. In order to guide the solar panel towards the north, a magnetometer HMC5883l was included in the planned solar tracker. The hybrid algorithm for solar tracking is depicted in Fig. 9 as a flow diagram.

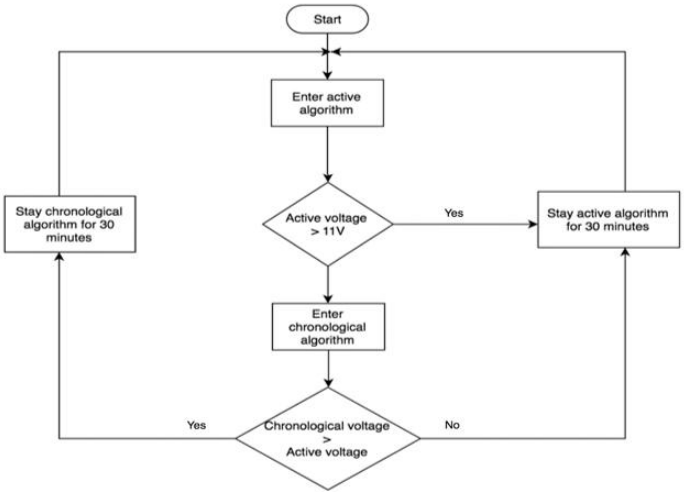

Fig- 9 Proposed hybrid algorithm.

4.3 Webpage for data monitoring

A webpage was established in addition to the solar tracker to allow for real-time monitoring of solar data, as seen in Fig. 9. The webpage was created using only basic HTML commands. The computer serves as a server, and SQLite was used to generate the database. A combination of SQLite commands and Mongoose format is used for server-database communication. The Arduino mega microcontroller and web browsers send queries to the server on a regular basis. When the server recognises the request, it retrieves the most recent solar data from the database in order to update the webpage's information.

V. EXPERIMENTAL RESULTS AND DISCUSSION

Real-world data was used to test the system. Because different panels from different manufacturers create varied amounts of power depending on the quality of the cells as well as the current produced, voltage output was chosen instead of the customary power in this study. However, we are focusing on the effect of irradiation on the panels as a direct result of their placement in relation to the sun. As a result, the open loop voltage is determined.

Real-world data was used to test the system. The output was first recorded against time for the entire day by positioning the PANEL midway between east and west with a tilt angle of roughly 26.8 south. Figure 8 depicts the reaction in static mode. It's easy to note that major electricity is only available for around five hours per day, from 10:30 to 15:30. By the end of May, this recording had been completed. Unfortunately, where the sun shines for around fourteen hours every day, this is insufficient. The same test was carried out again, but this time the PANEL was allowed to track the sun continually.

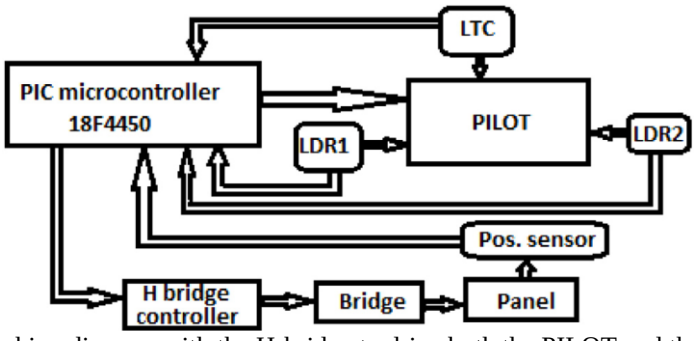

Fig- 8 Tracking diagram with the H-bridge to drive both the PILOT and the PANEL.

The tracking mode output is displayed in Fig. 9. The maximum extraction time has more than doubled, as can plainly be seen. That implies near maximum power extraction occurs from approximately an hour after sun rise until about an hour before sun set, when it becomes hotter and remains near maximum. By comparing the area beneath the two curves, it can be clearly inferred that the moving PANEL (continuous tracking) produces around 40% more energy than when it is stationary (static mode). Though this appears to be a significant improvement, this may not be the case. As previously stated, the continuous rotating PANEL has two fundamental drawbacks. Because the driving motor rotates at such a low speed, the machine may experience significant heat buildup and, more crucially, Because of the low rotational speed, the motor needs to draw a lot of current in order to provide enough torque to drive the PANEL. As a result, there is wasteful energy usage. In reality, it's possible that the amount of

energy spent exceeds the amount produced. Nothing is achieved if this is the case. The system was then put to the test, with the optimization technique being compared to the continuous mode. We got the result displayed in Fig. 10 by superimposing the two replies on the same graph. It shows that the extracted energy using the optimal approach is nearly the same as when the PANEL is continually rotating, while the consumed energy is significantly lower. It also demonstrates that the PANEL's number of movements is extremely limited throughout the day. In fact, just seven times at most, primarily at sunrise and sunset, when the sun's irradiation rapidly increases and declines. When the sun is shining brightly, it only takes three to five motions, but they must be made at large angles, such as 60 degrees. And this is just what is required.

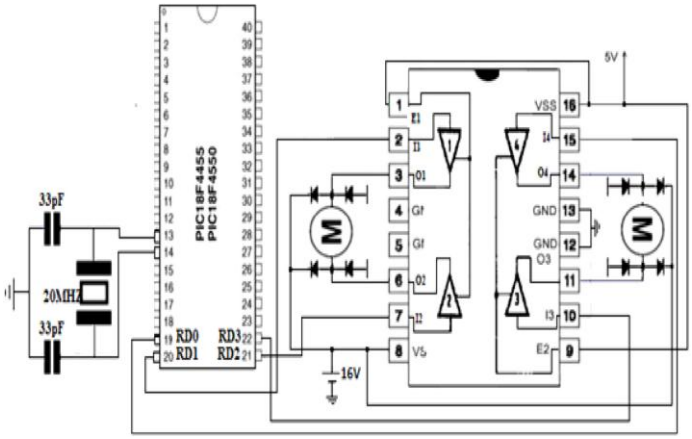

Fig- 10 Power drive to PANEL and PILOT motors.

As a result, the number of motor starts is highly limited, resulting in few beginning recurrence torques and a low current demand. It's worth noting that whether the sky is clear or foggy, or even wet, the system is unaffected because the relative comparison is the same in both circumstances, regardless of the irradiation intensity. Last but not least, the PANEL motor is extremely small, drawing only 10 milliamps. When compared to the PANEL's motor, this is insignificant. Even if thousands of panels are employed, just one PILOT is required to steer them all.

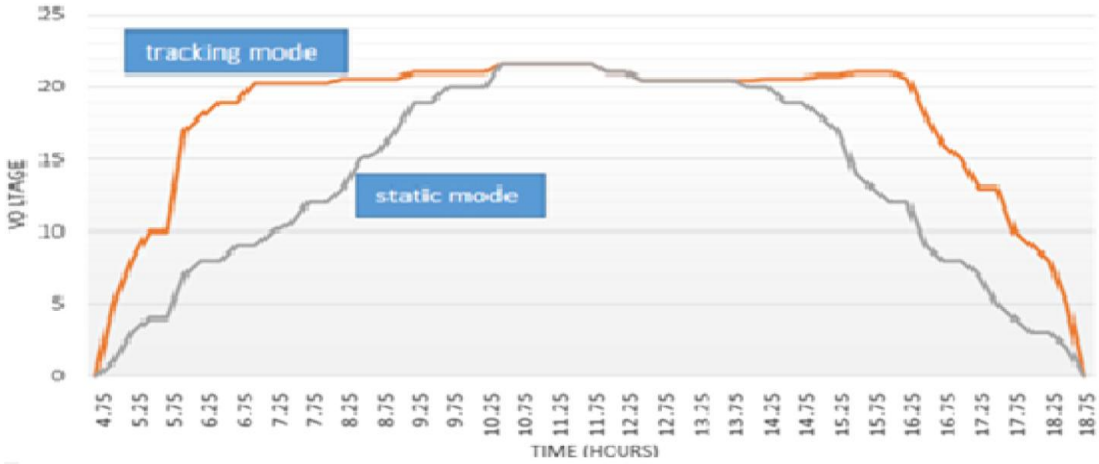

Fig- 12 Voltages for both stationary and moving PANEL.

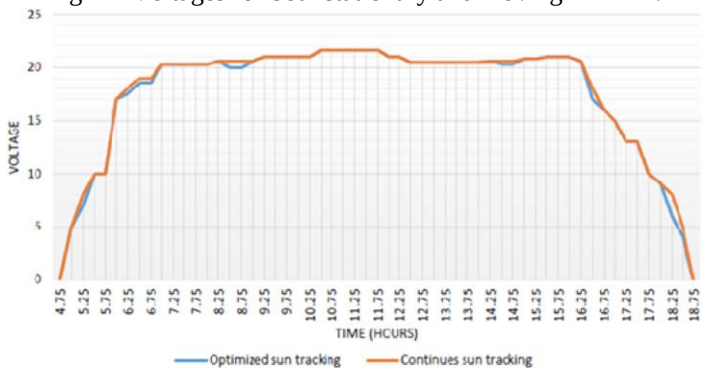

Fig- 13 Optimized tracking vs. continuous tracking.

VI. Discussion

Figure 11(a) depicts a model of the intended tracker, whereas Figure 11(b) depicts a photograph of the finished prototype. The control panel, which housed the microcontroller and motor driver, was the wooden box at the tracker's base. In the absence of batteries, the motor received power from a 24V power supply, while the microcontroller received power from a 5V power source. Red and green light emitting diodes (LEDs) were also included on the control panel to indicate the motor's status. The red LED turns on when there is no sunshine, and the green LED turns on when there is sunlight. When the solar tracker was turned on, it made the first movement to hourly movements after that first movement to obtain an average tilt for that hour.reach the needed angle of tilt for that particular time. It made

Fig- 11 (a) Model tracker; (b) Manufactured prototype

The electrical components in the design were precise and dependable, with a life expectancy of at least ten years. As they performed the commands of the intended software, these components were important in obtaining the performance indicated. The electronic components enabled the tracking, as evidenced by the changes in power output between the fixed and tracking panels depicted in Figure 10. The microcontroller determined the average hourly movement by calculating the amount of daylight hours for that particular day and the requisite degrees of movement. Figure 14 depicts the control panel, while Figure 12 depicts the result of the solar system's power output with and without the tracker. The load was a 24 ohm resistor linked to the solar panel output. Every 15 minutes, the voltage and current values between the two solar panels were measured, and the results were entered in an Excel spreadsheet.

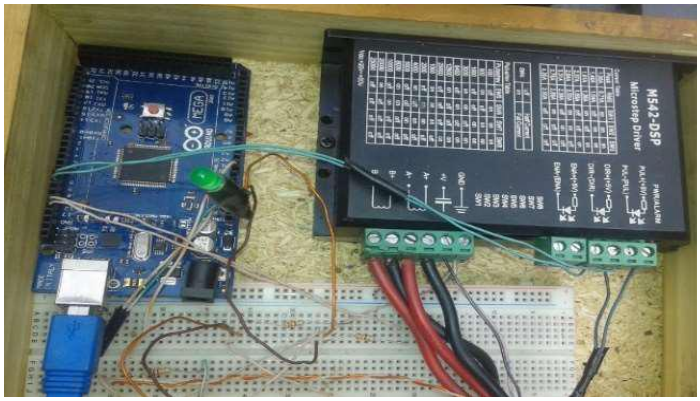

Fig- 14 Control panel

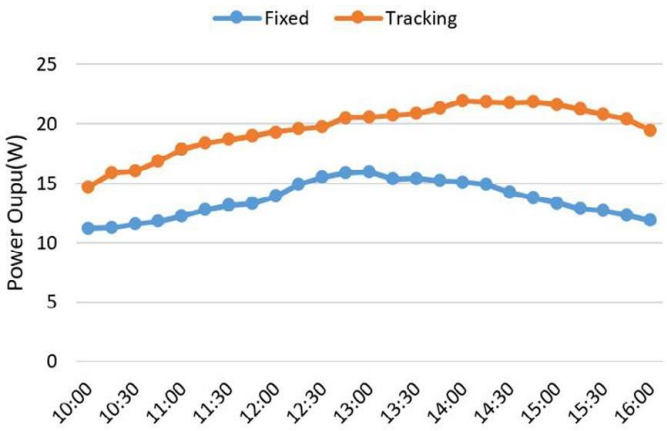

Fig- 15 Power output for a fixed panel and one with a tracker

The tracking programme was optimised by the use of meteorological data to train and simulate the controller's neural network under quickly changing conditions. The bill of materials for the designed solar tracker is shown in Table 1, along with estimated manufacturing costs. In comparison to the more complex solar trackers available, which vary from USD 1,000 and beyond for small ones of the same capacity and size found on Alibaba.com [21], the total cost of USD 147.4 was judged rather reasonable for such a simple system.

Table- 1 Bill of materials and cost of manufactured solar tracker

Item	Details	Quantity	Cost/USD
540x70 mm square tube	Mild steel	2	12
540x50 mm flat bar	Mild steel	1	2
86x137 mm metal sheet	Mild steel	4	15
53 mm square bar	Mild steel	1	6
42x20 mm round bar	Mild steel	2	9
Zinc plated 10x50 bolts	Mild steel	4	2
M10 zinc plated washers	Mild steel	2	0.4
SKF 61906 roller bearing	Mild steel	2	6
805x14 mm round tube	Mild steel	1	3
153x13 mm rectang. bar	Mild steel	1	2
Arduino Micro-controller	plastic	1	18
Fuji 24 volts stepper motor	copper	1	15
Light dependent resistor	silicon	1	1
M542-dsp motor driver	plastic	1	20
Pulley belt	rubber	1	5
10k resistor	silicon	1	1
Materials Cost			**117.4**
Approximate	Welding		10
Manufacturing Costs	Machining		15
Overheads			5
Total Cost			**147.4**

VII. Conclusions

It is possible to conclude that the proposed strategy maximises the amount of solar energy extracted. According to a comparison research, energy extraction increased by roughly 40% above fixed panels. The analysis also revealed that the optimised system has a significant advantage over a continually spinning panel. In fact, the energy savings on the consumption side were found to be just over 20%. More crucially, during peak hours, when the most energy is harvested, the panel spins only a few times (in this case, only three times). Furthermore, the scheme's attractiveness lies in the fact that hundreds of panels might be guided by a single tiny PILOT drawing very little current. As a general conclusion, with significant advancements in cell design, which are on the verge of reaching 50% efficiency, and a good optimum panel orientation, such as the one described here, which saves energy, the future of solar energy extraction appears quite promising indeed.

References

[1]. Best Research-Cell Efficiency Chart. NREL, 2019. [Online]. Available: https://www.nrel.gov/pv/cell-efficiency.html.
[2]. W.A. Badawy, A review on solar cells from Si-single crystals to porous materials and quantum dots, J. Adv. Res. 6(2) (2015) 123–132.
[3]. K. Yoshikawa, H. Kawasaki, W. Yoshida, T. Irie, K. Konishi, K. Nakano, T. Uto, D. Adachi, M. Kanematsu, H. Uzu, K. Yamamoto, Silicon heterojunction solar cell with interdigitated back contacts for a photoconversion efficiency over 26%, Nat. Energy 2(5) (2017) 17032.
[4]. R.W. MacQueen, M. Liebhaber, J. Niederhausen, M. Mews, C. Gersmann, S. Jäckle, K. Jäger, M.J. Tayebjee, T.W. Schmidt, B. Rech, K. Lips, Crystalline siliconsolar cells with tetracene interlayers: The path to silicon-singlet fission heterojunction devices, Mater. Horiz. 5(6) (2018) 1065–1075.
[5]. W. Shockley, H.J. Queisser, Detailed balance limit of efficiency of pn junction solar cells, J. Appl. Phys. 32(3) (1961) 510–519.
[6]. J. Benick, A. Richter, R. Müller, H. Hauser, F. Feldmann, P. Krenckel, S. Riepe, F. Schindler, M.C. Schubert, M. Hermle, A.W. Bett, High-efficiency n-type HP mc silicon solar cells, IEEE J. Photovolt. 7(5) (2017) 1171–1175.
[7]. F. Meillaud, A. Shah, C. Droz, E. Vallat-Sauvain, C. Miazza, Efficiency limits for single-junction and tandem solar cells, Sol. Energy Mater. Sol. Cells 90(18–19) (2006) 2952–2959.
[8]. M. Nayfeh, Advanced and low cost energy and lighting devices, Fundam. Appl. Nano Silicon Plasmonics Fullerines (2018) 363–429.
[9]. T. Matsui, K. Maejima, A. Bidiville, H. Sai, T. Koida, T. Suezaki, M. Matsumoto, K. Saito, I. Yoshida, M. Kondo, High-efficiency thin-film silicon solar cells realized by integrating stable a-Si:H absorbers into improved device design, Japanese J. Appl. Phys. 54(8S1) (2015) 08KB10.
[10]. M.A. Green, K. Emery, Solar cell efficiency tables (version 3), Prog. Photovolt. Res. Appl. 2(1) (1994) 27–34.
[11]. S. De Wolf, J. Holovsky, S.J. Moon, P. Löper, B. Niesen, M. Ledinsky, F.J. Haug, J.H. Yum, C. Ballif, Organometallic halide perovskites: Sharp optical absorption edge and its relation to photovoltaic performance, J. Phys. Chem. Lett. 5(6) (2014) 1035–1039.
[12]. Q. Jiang, Z. Chu, P. Wang, X. Yang, H. Liu, Y. Wang, Z. Yin, J. Wu, X. Zhang, J. You, Planar-structure perovskite solar cells with efficiency beyond 21%, Adv. Mater. 29(46) (2017) 1703852.
[13]. Oxford PV, Oxford PV Perovskite Solar Cell Achieves 28% Efficiency, 2018. [Online]. Available: https://www.oxfordpv.com/news/oxford-pv-perovskite-solarcell- achieves-28-efficiency. Accessed on: Apr. 16, 2019.
[14]. S.P. Philipps, F. Dimroth, A.W. Bett, High-efficiency III–V multijunction solar cells, in McEvoy's Handbook of Photovoltaics. Amsterdam, The Netherlands: Elsevier, 2018, pp. 439–472.
[15]. F. Dimroth, M. Grave, P. Beutel, U. Fiedeler, C. Karcher, T.N. Tibbits, E. Oliva, G. Siefer, M. Schachtner, A. Wekkeli, A.W. Bett, Wafer bonded four-junction GaInP/GaAs//GaInAsP/GaInAs concentrator solar cells with 44.7% efficiency, Prog. Photovolt. Res. Appl. 22(3) (2014) 277–282.
[16]. H. Helmers, O. Höhn, D. Lackner, E. López, L. Ruiz-Preciado, M. Schauerte, G. Siefer, F. Dimroth, A.W. Bett, Highly efficient III-V based photovoltaic laser power converter, in 1st Optical Wireless and Fiber Power Transmission Conf. (OWPT2019), no. OWPT-1-01, Yokohama, Japan, 2019.
[17]. J.F. Geisz, R.M. France, K.L. Schulte, M.A. Steiner, A.G. Norman, H.L. Guthrey, M.R. Young, T. Song, T. Moriarty, Six-junction III–V solar cells with 47.1% conversion efficiency under 143 Suns concentration, Nat. Energy 5(4) (2020) 326–335.
[18]. Luo Y, Zhang L, Wang X, Xie L, Liu ZB, Wu J, et al. A comparative study on thermal performance evaluation of a new double skin façade system integrated with photovoltaic blinds. Appl Energy 2017;199(8):281–93.
[19]. Hu Z, He W, Ji J, Hu DY, Lv S, Chen HB, et al. Comparative study on the annual performance of three types of building integrated photovoltaic (BIPV) Trombe wall system. Appl Energy 2017;194(5):81–93.
[20]. Li L, Qu M, Peng S. Performance evaluation of building integrated solar thermal shading system: building energy consumption and daylight provision. Energy Build 2016;113:189–201.
[21]. Jung HY, Kim KS. Control strategy of a venetian blind for visual improvement of work plane. J Archit Inst Korea 2010;26(12):279–86.
[22]. Huang Y, Niu JL, Chung TM. Comprehensive analysis on thermal and daylighting performance of glazing and shading designs on office building envelope in cooling dominant climates. Appl Energy 2014;134:215–28.
[23]. Koo SY, Yeo MS, Kim KW. Automated blind control to maximize the benefits of daylight in buildings. Build Environ 2010;45:1508–20.
[24]. Tzempelikos A. The impact of venetian blind geometry and tilt angle on view, direct light transmission and interior illuminance. Sol Energy 2008;82:1172–91.
[25]. Hong S, Choi AS, Sung M. Development and verification of a slat control method for a bi-directional PV blind. Appl Energy 2017;206(6):1321–33.
[26]. Roche L. Summertime performance of an automated lighting and blinds control system. Light Res Technol 2002;34:11–27.
[27]. Kim SH, Kim IT, Choi AS, Sung MK. Evaluation of optimized PV power generation and electrical lighting energy savings from the PV blind-integrated daylight responsive dimming system using LED lighting. Sol Energy 2014;107(9):746–57.
[28]. Kang H, Hong T, Jung S, Lee M. Techno-economic performance analysis of the smart solar photovoltaic blinds considering the photovoltaic panel type and the solar tracking method. Build Environ 2019;193(6):1–14.
[29]. Mousazadeh H, Keyhani A, Javadi A, Mobli H, Abrinia K, Sharifi A. A review of principle and sun-tracking methods for maximizing solar systems output. Renew Sustain Energy Rev 2009;13(8):1800–18.
[30]. Gao Y, Dong JF, Isabella O, Santbergen R, Tan H, Zeman M, et al. A photovoltaic window with sun-tracking shading elements towards maximum power generation and non-glare daylighting. Appl Energy 2018;228:1454–72.
[31]. Jayathissa P, Luzzatto M, Schmidli J, Hofer J, Nagy Z, Schlueter A, et al. Optimising building net energy demand with dynamic BIPV shading. Appl Energy2017;202(9):726–35.
[32]. T. Tudorache and L. Kreindler, Ed, "Design of a Solar Trackers system for pv power plants," *Acta plytechnica Hungarica*, Vol. 7, No 1, 2010.